Pure Appl. Geophys.

https://doi.org/10.1007/s00024-024-03527-8

Pure and Applied Geophysics

Mixed Topographic-Planetary Waves in a Stratified Ocean on a Background Flow

V. G. Gnevyshev,[1,2] V. S. Travkin,[1,3] and T. V. Belonenko[1]

Abstract—The work presents the development of Rhines' theory for mixed topographic-planetary waves in a stratified ocean on a background current. The vertical anisotropy of baroclinic Rossby waves has been established depending on the slopes of the topography. If for positive slopes (water shallowing to the north) the baroclinic mode node shifts downward, then for negative slopes the frequency and phase velocity decrease and the vertical node shifts upward. Estimates of frequency variability for vertical modes at a negative bottom slope were obtained. For weak changes in bottom topography in the long-wave limit, an analytical asymptotic expression of the dispersion relation for the surface mode is constructed for positive and negative slopes. The dispersion curves in one-dimensional and two-dimensional cases were analyzed numerically. It is shown that the range of influence of topography on baroclinic waves reaches maximum deviations of the order of 50% in the long-wave part of the spectrum.

Keywords: Planetary waves, Zonal flow, Doppler effect, Stratified ocean.

1. Introduction

The study of free quasi-geostrophic waves in a uniformly stratified ocean, where both topography and stratification are simultaneously considered, began with the work of Rhines (Rhines, 1970, 1977; Rhines & Bretherton, 1973). This foundational research was subsequently expanded upon by many authors (e.g., Charney and Flierl, 2007; Tailleux and McWilliams, 2001; Bobrovich and Reznik, 1999; Reznik & Tsybaneva, 1999; LaCasce, 2012, LaCasce, 2017).

The primary assumption in Rhines' analysis is the uniform slope of the topography, which permits the solution to be sought using separable variables. Qualitatively, the following scenario emerges: in the absence of topography, there exists a barotropic mode that is divergence-free under the 'solid lid' upper boundary condition, along with a countable set of baroclinic modes (Pedlosky, 1987; LeBlond & Mysak, 1981; Physics of the Ocean, 1978). Both barotropic and baroclinic modes are altered by topography in a complex manner.

With a negative slope $\delta < 0$, a barotropic mode exists. However, depending on the magnitude of the topographic slope, it can be conditionally divided into two waves: a fast barotropic mode (for small slopes) and a fast baroclinic mode (for large slopes δ). In this case, the usual baroclinic modes become slow baroclinic modes (Rhines, 1977). Rhines (1970) introduced the concept of baroclinic Rossby waves modified by bottom topography, referring to them as complementary *surface modes*. Rhines proposed a new term: if in his first work (Rhines, 1970) he called these waves 'surface waves', then in his next work (Rhines, 1977) he uses the term 'thermocline vortices' for them. Currently, the term 'surface modes' is used (LaCasce, 2017).

These analytical results gained particular significance after empirical data analyses in studies by Wunsch (1997), Samelson (1992), and LaCasce and Wang (2015). These studies showed that contrary to the scenario without topography where barotropic and first baroclinic modes are typically used, practical applications should instead consider modes that decay uniformly with depth, approaching zero near the ocean bottom. Wunsch (1997) termed these modes empirical orthogonal functions (EOF). Further research by de La Lama et al. (2016) revealed that the first empirical orthogonal function (EOF-1) is

[1] St. Petersburg University, 7–9, Universitetskaya nab., St. Petersburg 199034, Russia. E-mail: btvlisab@yandex.ru

[2] Shirshov Institute of Oceanology, Russian Academy of Sciences, 36 Nakhimovsky Prosp., Moscow 117997, Russia.

[3] N.N. Zubov's State Oceanographic Institute, Roshydromet, 6, Kropotkinskiy Lane, Moscow 119034, Russia.

Published online: 22 June 2024

predominant in extratropical regions, irrespective of bathymetry.

Further, LaCasce (2017) concludes that surface modes are ubiquitous in oceans, defining them as baroclinic modes emerging amidst substantial large-scale (rough) alterations in topography (slopes of the order of 10^{-2} are deemed sufficiently rugged for this classification). Perhaps the most intriguing insight from LaCasce's work is the suggestion that "a traditional barotropic regime probably does not exist," advocating instead for the conceptualization of topographic waves instead of barotropic Rossby waves.

It's noteworthy that in LaCasce's study (2017), an increase in the phase velocity of Rossby waves was observed for positive topography slopes. The author asserts that *the direction of the slope doesn't significantly impact the findings for most wave vectors*. This outcome has garnered significant attention as it diminishes the disparity between theoretical predictions for baroclinic Rossby waves over a flat seafloor and observational data from satellite-derived sea surface height (SSH) anomalies (Chelton and Schlax, 1996).

In this study, we do not explore the impact of bottom topography on unstable modes. Comprehensive investigations on this matter can be found in the works by Benilov (2001), Chen and Kamenkovich (2013), and LaCasce et al. (2018). It's essential to highlight an asymmetry between positive and negative topography slopes.

This work aims to numerically calculate vertical modes for surface waves, including their frequencies, phase and group velocities, for both positive and negative slopes, and to perform a qualitative and quantitative comparison. The analysis accounts for the background stationary zonal flow, ensuring that the constructed long-wave analytical asymptotics for the surface mode (the first baroclinic mode modified by topography) includes a classical Doppler shift.

2. Formulation of the Problem

The equations of planetary waves linearized against the background of a zonal stationary flow U in the Boussinesq and hydrostatics approximation have the form:

$$u_t + U\,u_x - fv + \frac{1}{\rho_*}p_x = 0, \tag{1}$$

$$v_t + U\,v_x + f\,u + \frac{1}{\rho_*}p_y = 0, \tag{2}$$

$$p_z = -\rho\,g. \tag{3}$$

Here u and v are the zonal and meridional velocity components, f is the Coriolis parameter, p is the hydrodynamic pressure,ρ_*- average density of the ocean, g – acceleration of free fall. The coordinate system is right-handed: the x-axis is directed to the east, the y-axis to the north, the z-axis is directed upward. For the density field $\rho = \rho_0(z) + \rho\,(x, y, z, t)$, $p_{0z} = -\rho_{0z}g$. The fluid is considered incompressible, therefore, the equation of conservation of mass breaks down into two equations for density and velocity.

The planetary wave Eqs. (1) – (3) are linearized against the background of a zonal stationary flow U in the β-plane approximation, while the system of equations is linearized not by some dimensionless parameter, such as the Rossby number, but by the amplitude factor. The solution is divided into the sum of the background flow, which has a conditional scale O (1), and certain small disturbances that have a certain small amplitude factor of the type $\varepsilon << 1$. In this case, only equations linear in ε are considered, in which the quadratic terms $\sim \varepsilon^2$ are eliminated.

If stratification is present, the equation for density can be written as follows:

$$\rho_t + U\,\rho_x - \frac{\rho_*}{g}N^2\,w = 0, \quad N^2 = -\frac{g}{\rho_*}\frac{d\rho_0}{dz}, \tag{4}$$

where N is the Väisälä-Brunt frequency (considered constant in this work). The continuity equation

$$u_x + v_y + w_z = 0 \tag{5}$$

Equations (1) – (5) are considered on the β-plane $f = f_0 + \beta y, f_0 = 2\Omega\sin\varphi_0$ is the doubled frequency of rotation of the Earth, Ω is the angular velocity of rotation of the Earth,$\beta = 2\Omega\cos\varphi_0/R$, where R is the radius of the Earth.

Similar to the approaches in Rhines (1970) and LeBlond & Mysak (1981), we define the topography changes as follows:

$$z = -H(y) = -H_0(1 - \delta y/L), \tag{6}$$

where δ is the slope and L is the width of the area where topography changes are observed.

In this formulation, there are two wave-forming parameters: the β-parameter, representing the latitudinal variation in the Coriolis parameter, and the topography gradient, which is specified as a parameter $\alpha = \frac{dz}{dy} = H_0\delta/L$. Following Rhines' logic, we consider both factors to have equivalent contributions, setting, setting $\alpha \sim 10^{-3}$ (LeBlond & Mysak, (1981). Taking $H_0 = 5 \times 10^3$ m, $L = 10^5$ m, we get δ = 10–2.

Let us use the 'rigid lid' condition as the upper kinematic boundary condition:

$$w = 0, \quad z = 0. \tag{7}$$

The topography is reflected in the kinematic boundary condition at the bottom—the impermeability condition:$(\vec{u} \cdot \vec{n}) = 0$, where $\vec{u} = (u, v, w)$ is the three-dimensional vector of the velocity field, $\vec{n}$ is the normal to the surface of the bottom topography h_b. Alternatively, the impermeability condition can be expressed as follows: $w_{bottom} = \vec{u} \cdot \nabla h_b$. Considering the notation adopted in Eq. (6), the impermeability condition at the lower boundary is expressed as:

$$w = \alpha v, \quad z = -H(y). \tag{8}$$

Note that in the monograph by Pedlosky (1987), an equation similar to Eq. (8) features a minus sign on the right side, stemming from a different method of specifying the lower boundary. According to Rhines () and LeBlond & Mysak (1981), the lower boundary is defined as $H = -H_0 + h(x, y)$. In Pedlosky's monograph (1987), bottom topography is presented in the form: $D = D_0 - h_b(x, y)$.

Next, following Rhines () and LeBlond & Mysak (1981), we proceed to dimensionless parameters:

$$\begin{aligned} (x, y) &= L(x', y'), \quad z = H_0 z', \quad t = f_0^{-1} t', \\ (u, v) &= U_0(u', v'), \quad w = (H_0 U_0/L)w', \\ p &= \rho_* U_0 f_0 L p', \quad \rho = (\rho_* U_0 f_0 L/g H_0)\rho'. \end{aligned} \tag{9}$$

The background state parameters are scaled as follows:

$$y = (L/\delta)y', \quad U = (L f_0)U'. \tag{10}$$

A comment: An unusual aspect of the nondimensionalization suggested by Rhines () is that while specifying the length scale L and the velocity field scale U_0, Rhines also defines the time scale f_0^{-1}. Typically, when length and time scales are defined, their ratio yields the velocity scale. However, Rhines takes a different approach in this regard.

Next, following Rhines and maintaining all scales for disturbances, we establish a new scale for the velocity field of the background flow and a meridional scale for the variability of the background state. From Eq. (1), we determine that the scale for the velocity field of the background flow should be defined as $f_0 L$ i.e. the last term in the second line of Eq. (10). This scale appears logical, representing the unit scale of the background flow velocity, while the disturbances during linearization are considered small-scale quantities.

Thus, two independent scales of the velocity field have emerged in the problem: U_0 for velocity field disturbances and $f_0 L$ for the background flow velocity field. Now we need to impose the condition that the background flow has a unit scale, and the scale of disturbances must be of the order of $\varepsilon << 1$. Then the condition is satisfied $U_0 << f_0 L$, which can be characterized as the smallness of the classical Rossby number $U_0/f_0 L \equiv Ro << 1$. The above reasoning confirms the validity of the nondimensionalization proposed by Charney and Flierl (2007).

Omitting the asterisks, we obtain dimensionless equations:

$$u_t + U u_x - \left(1 + \delta \overline{\beta} y\right) v + p_x = 0, \tag{11}$$

$$v_t + U v_x + \left(1 + \delta \overline{\beta} y\right) u + p_y = 0, \tag{12}$$

$$p_z = -\rho g, \tag{13}$$

where $\overline{\beta} = (\beta/f_0)(L/\delta) = \beta L/f_0 \delta$.

The problem involves two velocity scales: U_0 (for disturbances) and $f_0 L$ (background flow), along with two spatial scales: L (perturbation scale) and L/δ (background state scale in the meridional direction), formally derived by setting the depth to zero in (6).

For a more rigorous analysis, a zonal channel with two meridional walls is considered (Rhines, 1970), where the zonal channel width represents the L/δ scale. When reducing the disturbance quantities (u_x, u_y, p_x, v_x, v_y, p_y) to dimensionless form, the horizontal scale is set to L. For density, the equation is

$$\rho_t + U\rho_x - S^2 w = 0, \tag{14}$$

where $S^2 = N^2H^2/f^2L^2$ is Burger number, which we assume to be a constant value of the order of unity: for $N^2 = O(10^{-3})$ rad/s, $H_0 = 5 \times 10^3$ m, $L = 10^5$ m, we get $S \approx 1$.

The continuity equation

$$u_x + v_y + w_z = 0 \tag{15}$$

The lower boundary condition (8) can be rewritten as

$$w = \delta v, \quad z = -1 + \delta y. \tag{16}$$

Next, we look for a solution in the form of a plane wave $\exp[+i(kx + ly - \omega t)]$, where k and l are the zonal and meridional wave numbers, t is time, for definiteness the standard assumption that the frequency $\omega > 0$ is positive is accepted. Substituting into (11)–(16), we obtain

$$-i\,\omega_d\,u - \left(1 + \delta\,\overline{\beta}\,y\right)v + i\,k\,p = 0, \tag{17}$$

$$-i\,\omega_d\,v + \left(1 + \delta\,\overline{\beta}\,y\right)u + i\,l\,p = 0, \tag{18}$$

$$p_z = -\rho; \tag{19}$$

and for density

$$-i\,\omega_d\,\rho\, - S^2 w = 0. \tag{20}$$

where $\omega_d = \omega - k\,U$ is the Doppler frequency. The equation for the velocity field

$$i\,k\,u + i\,l\,v + w_z = 0 \tag{21}$$

The lower boundary condition (16) is left unchanged

$$w = \delta\,v, \quad z = -1 + \delta\,y. \tag{22}$$

Following the methodology outlined in (Rhines, 1970), we derive an asymptotic expansion with respect to the small parameter δ, which characterizes the influence of topography. It's worth noting that both topography and the β-parameter exert equal influence on wave propagation. These long waves, influenced by both factors, are referred to as 'mixed topographic-planetary waves'. Subsequently, we represent the physical fields (u, v, p, ρ) as asymptotic expansions given by:

$$u = u^{(0)} + \delta\,u^{(1)} + \ldots \tag{23}$$

We accept the low-frequency approximation $\omega_d << f$, filtering out internal waves and Kelvin waves (Rhines, 1970):

$$\omega_d = 0 + \delta\,\omega_d^{(1)} + \ldots \tag{24}$$

Substituting Eqs. (23), (24) into Eqs. (17)–(21) and organizing terms according to different powers of the small parameter δ, we derive the geostrophic equations for the zeroth order:

$$-v^{(0)} + i\,k\,p^{(0)} = 0, \tag{25}$$

$$u^{(0)} + i\,l\,p^{(0)} = 0, \tag{26}$$

$$p_z^{(0)} = -\rho^{(0)}, \tag{27}$$

$$w^{(0)} = 0, \tag{28}$$

$$i\,k\,u^{(0)} + i\,l\,v^{(0)} = 0. \tag{29}$$

In the first order of smallness (quasi-geostrophic) we obtain

$$-i\omega_d^{(1)}u^{(0)} - v^{(1)} - \delta\,\overline{\beta}\,y\,v^{(0)} + i\,k\,p^{(1)} = 0, \tag{30}$$

$$-i\omega_d^{(1)}v^{(0)} + u^{(1)} + \delta\,\overline{\beta}\,y\,u^{(0)} + i\,l\,p^{(1)} = 0, \tag{31}$$

$$p_z^{(1)} = -\rho^{(1)}, \tag{32}$$

$$-i\,w_d^{(1)} - S^2 w^{(1)} = 0, \tag{33}$$

$$i\,k\,u^{(1)} + i\,l\,v^{(1)} + w_z^{(1)} = 0. \tag{34}$$

Next, applying the classical procedure of velocity field reduction to the equations, we obtain the equation for pressure

$$w_d^{(1)}\left[S^{-2}p_{zz}^{(0)} - \left(k^2 + l^2\right)p^{(0)}\right] - \overline{\beta}\,k\,p^{(0)} = 0. \tag{35}$$

An alternative method to derive Eq. (35) is to linearize the nonlinear potential vorticity equation, as discussed in works by Pedlosky (1987) and LeBlond & Mysak (1981). This linearization involves decomposition with respect to the Rossby number

(small parameter), as outlined by Charney & Flierl (2007).

The upper boundary condition is the 'solid lid' approximation:

$$p_z^{(0)} = 0, \quad z = 0. \tag{36}$$

The lower boundary condition is the impermeability condition:

$$\omega_d^{(1)} p_z^{(0)} = S^2 k\, p^{(0)}, \quad z = -1. \tag{37}$$

The desired frequency $\omega^{(1)}$ is included both in the differential equation and in the lower boundary condition.

2.1. Surface Mode

We refer to the first baroclinic mode, modified by topography, as the 'surface mode', following the terminology used in studies by Rhines (1970) and LaCasce (2017). The solution that meets Eq. (35) and the upper boundary condition (36) is expressed as $p^{(0)} = \cos mz$. Substituting it into Eq. (35), we get

$$\omega_d^{(1)} = \frac{-\overline{\beta}\, k}{k^2 + l^2 + m^2/S^2}. \tag{38}$$

Substituting $p^{(0)} = \cos m\, z$ into the lower boundary condition (37), we obtain the eigenvalue equation

$$\omega_d^{(1)}\, m \tan m = k\, S^2. \tag{39}$$

From (38) and (39), we obtain

$$\overline{\beta}\, m \tan m = -\left[\left(k^2 + l^2\right)S^2 + m^2\right]. \tag{40}$$

We will interpret this equation as the relationship between the vertical eigenvalue m and the horizontal wave number k : i.e. $m = m(k^2 + l^2)$. A graphical analysis of Eq. (40) is presented in Fig. 1. In the absence of topography ($\delta = 0$), the eigenvalue m does not depend on the wave number, and for the first baroclinic mode $m = \pi$ is the first non-zero root of the equation $\tan m = 0$. The vertical eigenvalue for the surface mode is in the range $\pi/2 < m_1 < \pi$, that is, lies to the left of the point $m = \pi$, with a positive slope $\delta > 0$. With a negative bottom slope $\delta < 0$, the eigenvalue lies in the interval $\pi < m_1 < 3\pi/2$.

An example of a numerical solution of these equations taking into account the limits of changes in

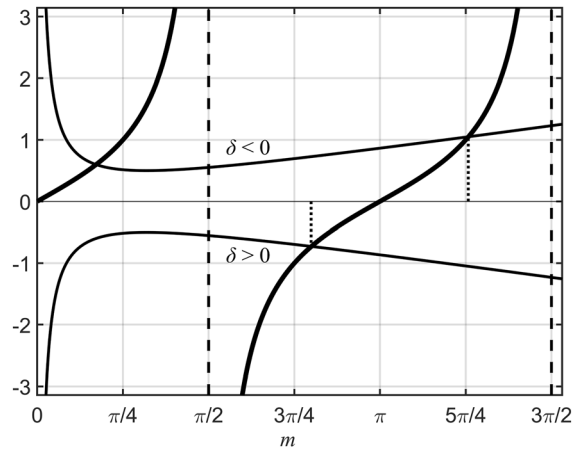

Figure 1
Graphical solution of Eq. (40) for the surface mode. With a positive $\delta > 0$ and a negative slope of the bottom $\delta < 0$

the frequency of the surface mode is shown in Fig. 2. It is worth paying attention to how quickly the surface mode with negative slopes (dashed line with a dot) tends to its lower limit (lower black thin line).

The analytical expression for the zonal component of group velocity (excluding the Doppler shift) is as follows:

$$C_{gx} = \omega_k = \frac{-\overline{\beta}\,\left(m^2 + l^2 - k^2 - 2\, m\, k\, m_k\right)}{\left(k^2 + l^2 + m^2\right)^2}, \tag{41}$$

where

$$m_k = \frac{-2\, k}{\overline{\beta}\,\left[\tan m + m(\tan^2 m + 1)\right] + 2\, m}. \tag{42}$$

The last expression is obtained by differentiating the ratio (40) (see Gnevyshev et al., 2023a, b).

For the meridional component of the group velocity, we have

$$C_{gy} = \omega_l = \frac{-2\,\overline{\beta}\, k\,(l + m\, m_l)}{\left(k^2 + l^2 + m^2\right)^2}, \tag{43}$$

where

$$m_l = \frac{-2\, l}{\overline{\beta}\,\left[\tan m + m(\tan^2 m + 1)\right] + 2\, m}. \tag{44}$$

The outcome of the numerical computation for phase and group velocities in the one-dimensional case ($l = 0$) is depicted in Fig. 3. It is evident from the graph that the most significant deviations of the

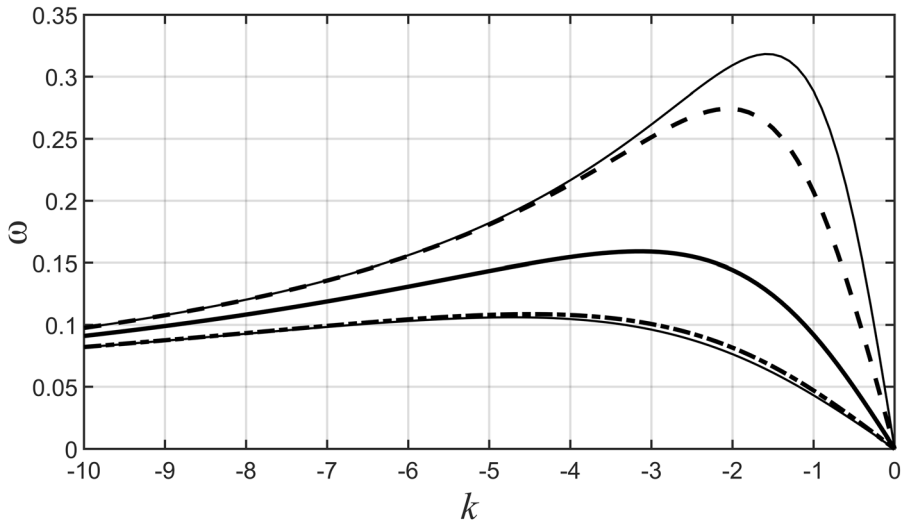

Figure 2
Frequency of the first baroclinic mode (black bold line). The boundaries of the frequency change of the surface mode are shown by a thin black line: the upper one for positive slopes) and the lower one for negative ones. The frequency of the surface mode with a positive slope (black dotted line) when $\overline{\beta} = 1$; $S = 1$; $l = 0$, and a negative slope (black dotted line with a dot) when $\overline{\beta} = -1$; $S = 1$; $l = 0$

surface mode from the first baroclinic mode happen with positive topography slopes. The point of inflection (where the group velocity crosses zero) moves towards the domain of long waves for positive slopes and towards the domain of short waves for negative slopes.

Figure 4 illustrates the outcome of the numerical computation of the vertical eigenvalues. The asymptote $m = \pi$ represents a purely baroclinic mode. Comparing Fig. 4 with Fig. 1 by LaCasce (2017), it is apparent that the transition from a model with constant stratification to one with exponential stratification results in quantitative rather than qualitative changes. The horizontal asymptotics of the eigenvalues are approaching each other. The asymptote $m = \pi$ shifts down to the value of 2.76, and the lower asymptote $m = \pi/2$, on the contrary, moves up to the value of 2.41.

The calculation of the vertical eigenfunction is depicted in Fig. 5. Figure 5a shows that for positive slopes, the result is a displacement of the node downwards in the direction of the bottom (this is a classic well-known result). For negative slopes (Fig. 5b), on the contrary, the node rises. This is a qualitatively new result obtained in this work. Until now, it was believed that the direction of the topographic slope was not significant, leading to the consideration of only positive slopes.

Isolines of dispersion surfaces are shown in Fig. 6. For a positive slope (Fig. 6a), a pure baroclinic mode is shown on the left. The dotted line marks the isolines of the surface mode, the graph of which is shown in the center in Fig. 6. The graph on the right side of Fig. 6a is the distribution of the vertical eigenvalue m depending on the wave numbers k and l; there is a maximum in the center of the figure. From Fig. 6a it is clear that the extremum (cutoff frequency) increases in magnitude and shifts towards longer waves with a positive slope. For negative slopes (Fig. 6b), the extremum, on the contrary, shifts towards short waves and decreases in magnitude; there is a minimum in the center of the figure characterizing the distribution of the vertical eigenvalue m depending on the wave numbers k and l.

Figure 7 illustrates the two-dimensional zonal group velocity field. In the center, baroclinic mode. To the left of it (leftmost figure) is the surface mode with a positive slope, and to the right (far right figure) is the surface mode with a negative slope. It can be seen that all three distributions have a common

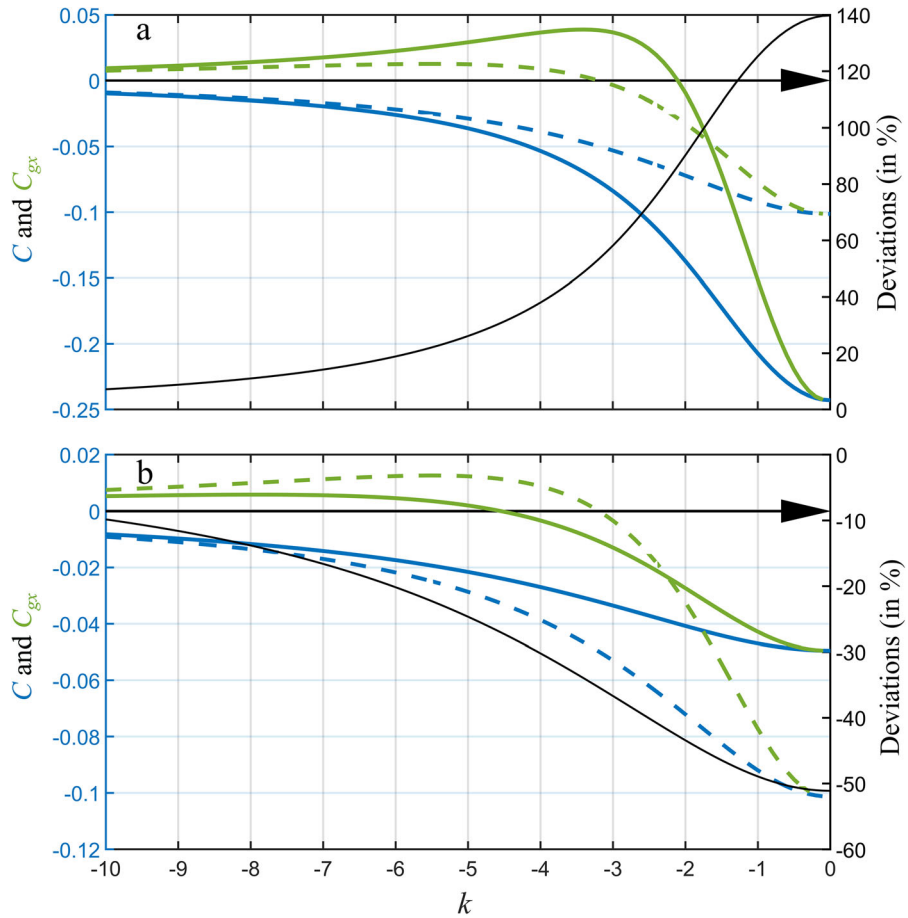

Figure 3
Phase velocity C (blue) and group velocity C_{gx} (green) of the first baroclinic mode (dotted line) and surface mode (solid line) when $\overline{\beta} = 1$; $S = 1$; $l = 0$ (**a**), and $\overline{\beta} = -1$; $S = 1$; $l = 0$ (**b**). The black thin line shows the deviation (in %) of the phase velocity of the surface mode from the phase velocity of the baroclinic mode

structure, but differ numerically. Notably, the zonal group velocity has two extrema.

Figure 8 displays the field of the meridional component of the group velocity. In the center is the baroclinic mode, on the left is the surface mode with a positive slope δ, and on the right is the surface mode with a negative slope δ. Notably, the extremum of the meridional component of the group velocity always lies on the bisector of the angle in wave space (k, l). This observation is supported by examining formulas (40), (43), and (44), as they exhibit symmetry for wave numbers, a characteristic shared by both the baroclinic and surface modes.

2.2. *Long-Wavelength Asymptotics of the Surface Mode*

Even though there are no obstacles for numerical calculations, for physical understanding it is useful to find analytically the asymptotic behavior in the long-wave limit.

For a baroclinic wave (refer to Fig. 3), we approximate the tangent function with a Taylor series, considering only the first few terms in the vicinity of $m = \pi$. Consequently, condition (40) can be expressed as:

$$\overline{\beta}\, m(m-\pi) = -\left[\left(k^2+l^2\right)S^2 + m^2\right]. \qquad (45)$$

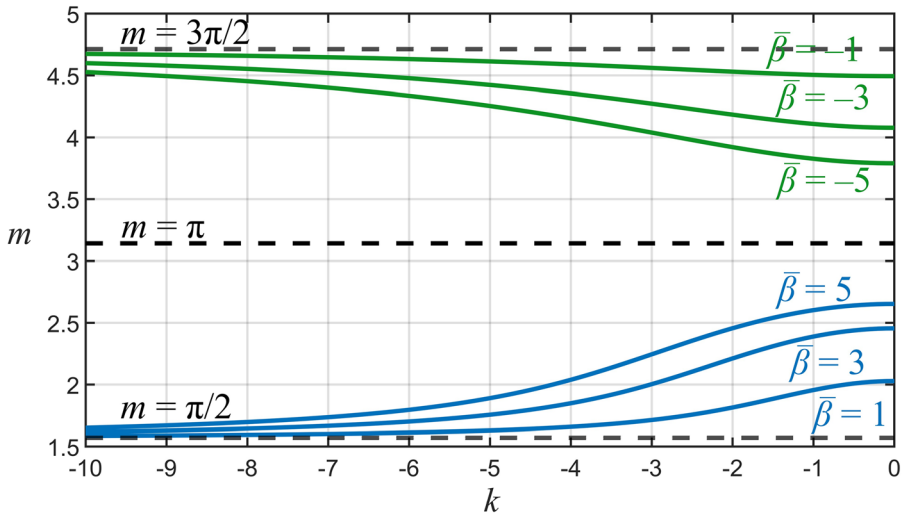

Figure 4
Dependence of the eigenvalues m of the first baroclinic topographic mode on the wave number k when $\overline{\beta} = 1, 3, 5$ (blue color), and when $\overline{\beta} = -1, -3, -5$ (green color). Dotted lines are $m = \pi/2$, $m = \pi$, and $m = 3\pi/2$

Opening the bracket on the left side and setting $m \sim \pi$, we replace $\overline{\beta}\,\pi\,m$ on $\overline{\beta}\,\pi^2$, where we find

$$m^2 = \frac{\overline{\beta}\,\pi^2 - S^2(k^2 + l^2)}{\overline{\beta} + 1}. \tag{46}$$

Next, we solve for m^2 from Eq. (38), and considering (46) and (24), we derive the asymptotic expression for the first baroclinic mode along with its validity limits:

$$\omega = \frac{-(\beta + \alpha)k}{k^2 + l^2 + \pi^2/S^2} + kU; \quad |\alpha| << \beta; \quad k^2 + l^2 << \beta\,\pi^2/S^2. \tag{47}$$

The second condition implies that the topographic variations are minor, but the crucial factor is the magnitude of the slope angle. This indicates that the asymptotic approximation is applicable for both positive (where water shallows to the north) and negative (where water shallows to the south) values of the bottom slope α. In the former scenario, the topography amplifies the β-effect, while in the latter, it diminishes it. Let us recall that the relative smallness of topographic slopes in middle latitudes gives the condition for slope angles $|\alpha| << 10^{-3}$. The final condition in the asymptotic expression (47) signifies the long-wavelength approximation. It's essential to highlight that this expression, on one hand, illustrates how the bottom slope, causing either vortex stretching or compression, acts as an effective $\overline{\beta}$, depending on $(\beta + \alpha)$. However, it's crucial to recognize that this direct combination of effects is valid only for small slopes and exclusively in the long-wave regime. As the topographic slope increases, the mode, upon reaching a certain threshold, ceases to respond significantly to further changes in the topographic angle. For higher numbers of baroclinic modes, generalization occurs according to the principle $(\pi)^2$ goes into $(\pi\,n)^2$.

3. Discussion and Conclusions

In this study, we highlight an asymmetry between positive and negative topography slopes. Formally, the limit points for positive and negative slopes coincide, yet their approach to these limits differs, illustrating an asymmetry in topography slope signs. With a positive slope (shallow water to the north), there is no barotropic mode, and the accumulation point for the first baroclinic mode is on the left. As the topography slope increases, the vertical wave number shifts leftward from π to $\pi/2$ (refer to Fig. 1). Concurrently, the frequency and phase velocity increase, maintaining upper limits. Conversely, for

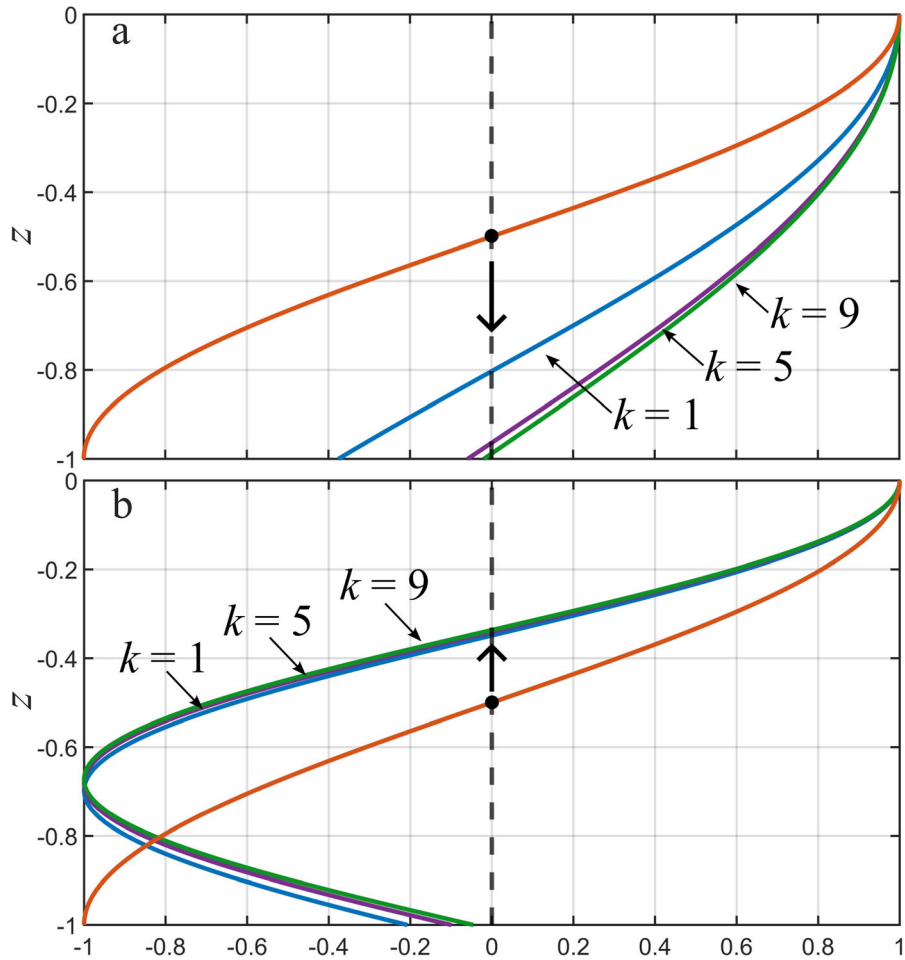

Figure 5
Vertical Z modes of the surface wave when $\overline{\beta} = 1$ (**a**) and $\overline{\beta} = -1$ (**b**); $S = 1$; $k = 1, 5, 9$; $-1 < Z < 0$. The orange color shows the first baroclinic mode in the absence of topography

negative slopes (δ), the accumulation point of the first baroclinic mode shifts to the right, from π to $3\pi/2$. In this scenario, frequency and westward-directed phase velocity decrease limited already from below. Additionally, the vertical mode node ascends instead of descending. In this case, the missing limiting eigenvalue $\pi/2$ is replaced by a barotropic (fast baroclinic) mode, which is absent with a positive slope δ.

Thus, we argue that the frequency and westerly component of the phase velocity of the topography-modified first baroclinic mode can either increase ($\delta > 0$) or decrease ($\delta < 0$) depending on the sign of the topography slope. Similarly, a vertical node can either move down ($\delta > 0$) or rise ($\delta < 0$). Based on our numerical analysis, we conclude that the influence of topography on the westerly propagation of Rossby waves is somewhat exaggerated. Note that the result regarding the asymmetry of positive and negative slopes aligns with the findings of Colin de Verdière (2005) with a piecewise constant shear velocity of the background flow. It was found that there is an increase (or decrease) in the westerly component of the phase velocity when the surface mean flow is directed east (or west), while the dimensionless number R^2 characterizes the ratio of the topographic slope to the beta parameter.

The primary findings of this study can be summarized as follows:

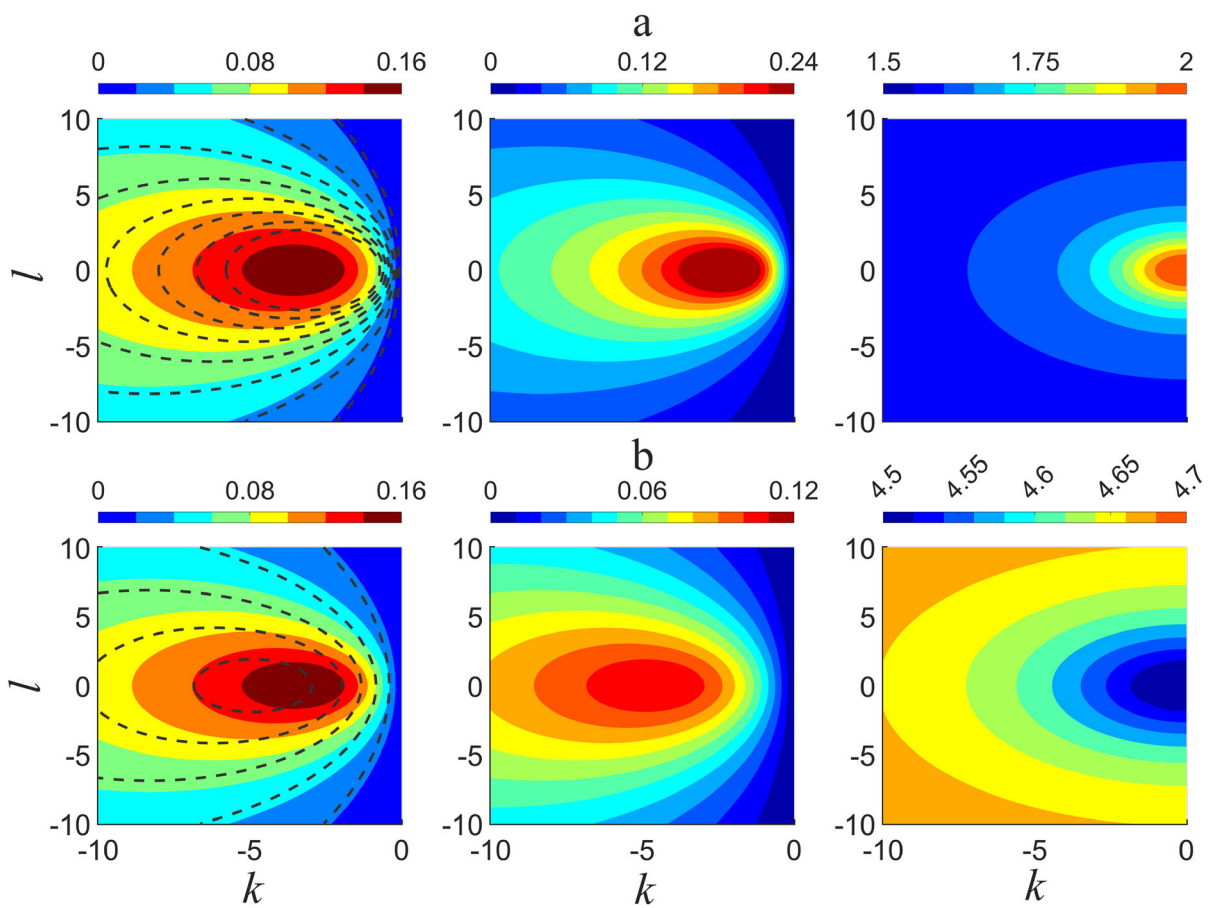

Figure 6
Frequency of the first baroclinic mode (left), surface mode (center), and vertical eigenvalue (right): **a** with a positive slope ($\overline{\beta} = 1$; $S = 1$); **b** with a negative slope ($\overline{\beta} = -1$; $S = 1$)

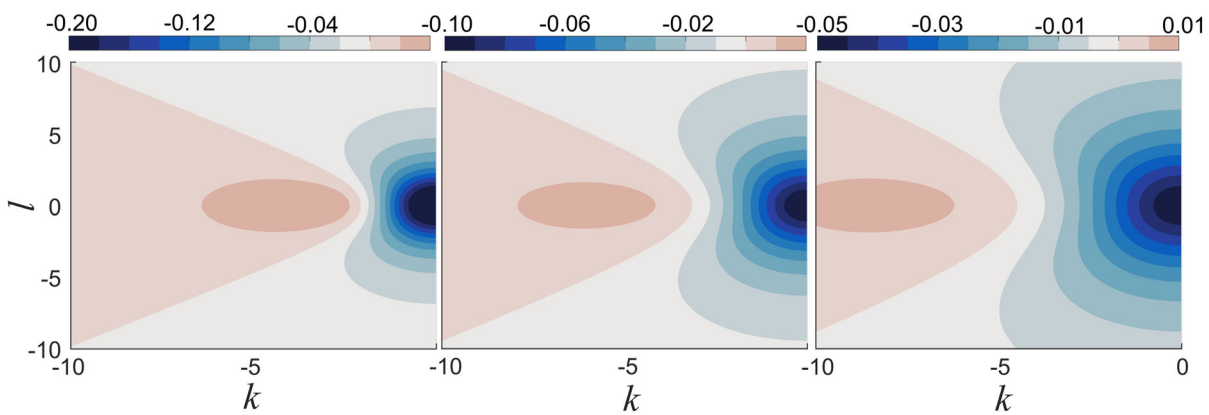

Figure 7
The zonal component of the group velocity of the first baroclinic mode (in the center) and the surface mode (on the left) at $\overline{\beta} = 1$ and at $\overline{\beta} = -1$ (on the right)

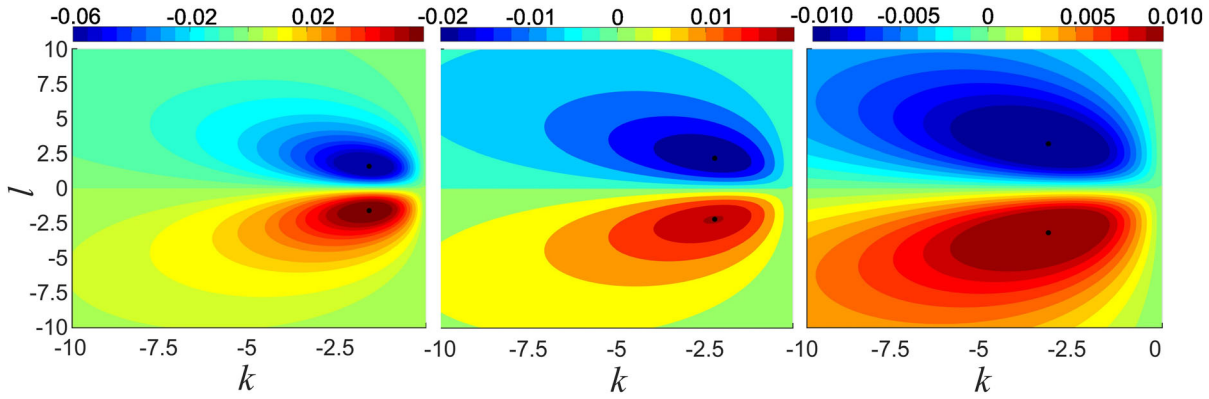

Figure 8
The meridional component of the group velocity of the first baroclinic mode (in the center) and the surface mode at $\overline{\beta} = 1$ (on the left) and at $\overline{\beta} = -1$ (on the right). The extremum is reached at values (k, l): ($-$ 1.6, $\pm$ 1.6) – the graph on the left; ($-$ 2.2, $\pm$ 2.2) – the graph on the center; ($-$ 3.2, $\pm$ 3.2) – the graph on the right

1. We extended Rhines' asymptotic theory to encompass mixed topographic-planetary waves in a stratified ocean under the influence of a background flow. Analysis of scales revealed the need to incorporate the characteristic velocity scale of the background flow fL, and the meridional scale of topographic variability L/δ (see Eq. (10)). As a consequence, an additional dimensionless small parameter appears in the analysis – the Rossby number U/fL, the smallness of which is crucial for linearizing the equations (Charney and Flierl, 2007).

2. The well-known statement about the limitation of the frequency range of baroclinic Rossby waves from *above* by an ocean of double effective thickness (Rhines, 1970; Bobrovich and Reznik 1999) as well as the downward shift of the baroclinic mode node is not entirely correct. We have established that this statement is true only for positive slopes (water shallowing to the north). For negative slopes, on the contrary, the frequency and phase velocity decrease, and the vertical node does not descend, but, on the contrary, rises. The frequency estimate from below is obtained at an effective ocean depth of $2/3H$ for the first baroclinic mode with a negative slope. This is easy to understand based on the following simple reasoning. If for positive slopes the vertical wavenumber m decreases in the direction $\pi/2$ (accumulation point on the left), then the vertical phase increment at ocean depth mH also decreases and the node descends. For negative slopes, the opposite happens, the accumulation point is located on the right, and the phase increment increases. There is anisotropy in the direction of the bottom slope (north–south). This anisotropy becomes more understandable if positive slopes are replaced by eastward currents and negative slopes by westward currents (Colin de Verdière 2005; LaCasce et al., 2018).

3. For minor alterations in bottom topography, analytical asymptotics of the dispersion relation for the surface mode (47) are derived for both positive and negative slopes. It's worth noting that similar asymptotics were developed for the topographic mode with a positive slope (Pedlosky, 1987), and for the barotropic mode with a negative bottom slope (Rhines, 1977).

4. Dispersion curves were numerically analyzed when the meridional component of the wave number $l = 0$, as well as two-dimensional dispersion curves, phase and group velocities at $l \neq 0$. From the analysis performed, it follows that the range of influence of topography on baroclinic waves reaches maximum deviations of the order of 50% in the long-wave part of the spectrum. For positive slopes, group and phase velocities increase, and for negative slopes they decrease.

Acknowledgements

The research was carried out with the support of St. Petersburg University, grant No. 116442164, and within the framework of the state assignment of the Institute of Oceanology of the Russian Academy of Sciences No. FMWE-2024-0017.

Author contributions V.G. and T.B. wrote the main manuscript text and V.T. prepared figures 1-8. All authors reviewed the manuscript

Funding

The authors have not disclosed any funding.

Data Availability

No datasets were generated or analysed during the current study.

Declarations

Conlfict of interest The authors declare no competing interests.

References

Benilov, E. S. (2001). Baroclinic instability of two-layer flows over one-dimensional bottom topography. *Journal of Physical Oceanography., 31*, 2019–2025. https://doi.org/10.1175/1520-0485(2001)031%3c2019:BIOTLF%3e2.0.CO

Bobrovich, A. V., & Reznik, G. M. (1999). Planetary waves in a stratified ocean of variable depth Part 2. Continuously stratified ocean. *Journal of Fluid Mechanics., 388*, 147–169. https://doi.org/10.1017/S0022112099004863

Charney, J. G., and G. R. Flierl. (2007). Oceanic Analogues of Large-Scale Atmospheric Motions, Jule G. Charney and Glenn R. Flierl, pp. 504–549. https://ocw.mit.edu/courses/res-12-000-evolution-of-physical-oceanography-spring-2007/pages/part-4/

Chelton, D., & Schlax, M. (1996). Global observations of oceanic Rossby waves. *Science, 333*(272), 234–238. https://doi.org/10.1126/science.272.5259.234

Chen, C., & Kamenkovich, I. (2013). Effects of topography on baroclinic instability. *Journal of Physical Oceanography, 43*, 790–804. https://doi.org/10.1175/JPO-D-12-0145.1

Colin de Verdière, A., & Tailleux, R. (2005). The Interaction of a Baroclinic mean flow with long rossby waves. *Journal of Physical Oceanography, 35*(5), 865–879. https://doi.org/10.1175/jpo2712.1

de La Lama, M. S., LaCasce, J. H., & Fuhr, H. (2016). The vertical structure of ocean eddies. *Dynamics and Statistics of the Climate System, 1*, dzw001. https://doi.org/10.1093/climsys/dzw001

Gnevyshev, V. G., Travkin, V. S., & Belonenko, T. V. (2023a). Topographic factor and limit transitions in the equations for subinertial waves. *Fundamental and Applied Hydrophysics., 16*(1), 8–23. https://doi.org/10.48612/fpg/92rg-6t7h-m4a2

Gnevyshev, V. G., Travkin, V. S., & Belonenko, T. V. (2023b). Group velocity and dispertion of Buchwald and Adams shelf waves: A new analytical approach. *Fundamental and Applied Hydrophysics, 16*(2), 8–20. https://doi.org/10.59887/2073-6673.2023.16(2)-1. (in Russian).

LaCasce, J. H. (2012). Surface quasigeostrophic solutions and baroclinic modes with exponential stratification. *Journal of Physical Oceanography, 42*, 569–580. https://doi.org/10.1175/JPO-D-11-0111.1

LaCasce, J. H. (2017). The prevalence of oceanic surface modes. *Geophysical Research Letters, 44*, 11097–11105. https://doi.org/10.1002/2017GL075430

LaCasce, J. H., Escartin, J., Chassignet, E. P., & Xu, X. (2018). Jet instability over smooth, corrugated and realistic bathymetry. *Journal of Physical Oceanography*. https://doi.org/10.1175/JPO-D-18-0129.1

LaCasce, J. H., & Wang, J. (2015). Estimating subsurface velocities from surface fields with idealized stratification. *Journal of Physical Oceanography, 45*, 2424–2435. https://doi.org/10.1175/JPO-D-14-0206.1

LeBlond P.H., Mysak L.A. (1981). Waves in the Ocean. Elsevier Oceanography Series, Volume 20. 602 pp.

Physics of the ocean. Vol. 2. Ocean hydrodynamics. (1978). Ed. Kamenkovich V.M., Monin A.S. M., Nauka, 455 p.

Pedlosky J. (1987). Geophysical fluid dynamics. Springer Verlag, New York, 710 p. https://doi.org/10.1007/978-1-4612-4650-3.

Reznik, G. M., & Tsybaneva, T. B. (1999). Planetary waves in a stratified ocean of variable depth. Part 1. Two-layer model. *Journal of Fluid Mechanics., 1999*(388), 115–145. https://doi.org/10.1017/S0022112099004875

Rhines, P. (1970). Edge-, bottom-, and Rossby waves in a rotating stratified fluid. *Geophysical and Astrophysical Fluid Dynamics, 1*, 273–302. https://doi.org/10.1080/03091927009365776

Rhines, P.B. (1977). The dynamics of unsteady currents, in The Sea, vol. 6, E.D. Goldberg ed., Wiley Interscience, N.Y., 189–319.

Rhines, P. B., & Bretherton, F. (1973). Topographic Rossby waves in a rough-bottomed ocean. *Journal of Fluid Mechanics, 61*, 583.

Samelson, R. M. (1992). Surface-intensified Rossby waves over rough topography. *Journal of Marine Research, 50*, 367–384. https://doi.org/10.1357/002224092784797593

Tailleux, R., & McWilliams, J. C. (2001). The effect of bottom pressure decoupling on the speed of extratropical, baroclinic Rossby waves. *Journal of Physical Oceanography, 31*(425), 1461–1476. https://doi.org/10.1175/1520-0485(2001)031%3c1461:TEOBPD%3e2.0.CO;2

Wunsch, C. (1997). The vertical partition of oceanic horizontal kinetic energy. *Journal of Physical Oceanography, 27*, 1770–1794. https://doi.org/10.1175/1520-0485(1997)027%3c1770:TVPOOH%3e2.0.CO;2

(Received May 20, 2024, revised May 20, 2024, accepted June 17, 2024)